"PROCESS": Systems studies of spherical tokamaks

Stuart I. Muldrew[a,*], Hanni Lux[a], Geof Cunningham[a], Tim C. Hender[a], Sebastien Kahn[a], Peter J. Knight[a], Bhavin Patel[a,b], Garry M. Voss[a], Howard R. Wilson[a,b]

[a] *Culham Centre for Fusion Energy, UK Atomic Energy Authority, Culham Science Centre, Abingdon, Oxfordshire OX14 3DB, UK*
[b] *York Plasma Institute, Department of Physics, University of York, Heslington, York YO10 5DD, UK*

ARTICLE INFO

ABSTRACT

With a reduced aspect ratio, spherical tokamaks have a number of attractive features for a fusion power plant. This can be studied using systems codes, which allow for the rapid conceptual study of power plants covering everything, from the plasma through to electricity generation. In this paper, we describe models in the systems code PROCESS that have been added specifically for spherical tokamaks. Within PROCESS an alternative relation for the plasma current is included which accounts for the increased ratio of I_p/aB. We have tested this against a series of equilibria created with the free boundary equilibrium code FIESTA, and additionally performed our own fit. We also outline the engineering changes that can be made to the device and describe a water-cooled copper centrepost model. To test our models we recreate the published designs for the Fusion Nuclear Science Facility (FNSF) and a High Temperature Superconducting Pilot Plant (HTS-PP) and find good agreement. We conclude by highlighting the efficiencies needed to produce net electricity from small fusion devices.

1. Introduction

Spherical tokamaks offer a number of potential advantages for a future fusion power plant. They have a high ratio of thermal-to-magnetic field pressure (β) and strong flows, either of which could result in reduced turbulence. Fewer toroidal field coils and a different geometry offers the potential for new methods of remote maintenance and lower magnet costs. (For more information see review articles e.g. [1,2]).

Systems codes can be employed to scope out parameter space quickly by using a set of simplified, yet comprehensive, models to rapidly determine feasible tokamak designs. Spherical tokamaks have a number of differences compared with their conventional aspect ratio counterparts, and in this paper we present the spherical tokamak specific models implemented in the systems code PROCESS. PROCESS has previously been used extensively to study conventional aspect ratio devices such as EUROfusion-DEMO [3], CFETR [4] and SST-2 [5].

To model spherical tokamaks an alternative relation between the plasma current and the ratio of the toroidal magnetic field to the safety factor is implemented, to account for an increased ratio of I_p/aB that can be accommodated at low aspect ratio. This is driven by the strongly enhanced toroidal rotation that gives a higher plasma current for a given safety factor [6]. We also include the contribution of the diamagnetic current to the overall plasma current, which is higher than in a conventional aspect ratio device due to the higher β and the field line

pitch. Various options are available to alter the build of the device; these include the ability to remove the central solenoid and avoid inboard breeding blankets, to join the TF coils into a single centerpost, to reposition the shaping poloidal field coils within the TF coils, and to increase the divertor space. These design modifications are aimed at overcoming the challenges presented, such as the limited inboard space and the increased divertor heat loads, however will impact start-up and the tritium breeding ratio.

The rest of this paper is structured as follows. In Section 2 we describe the spherical tokamak specific models within PROCESS in detail and then in Section 3 we apply them to two examples from the literature. We conclude in Section 4. Throughout this work we are using PROCESS version tag: 1.0.16-300-g470be046.

2. Spherical tokamak models in PROCESS

The physics and engineering models in PROCESS have previously been described in [7,8]. These papers cover the models that are used for conventional aspect ratio tokamaks. A number of spherical tokamak specific models have also been developed, principally based on [6,9–11]. Here we give an overview of these models with further details available in the references.

2.1. Inboard radial build

One of the challenges of spherical tokamaks is the limited space on the inboard side to fit all the components into. To alleviate this, an alternative inboard build can be adopted. The primary difference is that the toroidal field coils all join onto a single centrepost that runs through the centre of the device. This carries all of the current and takes less space than individual limbs. The centrepost is hollow at the centre to accommodate a central solenoid (see figure 5 of [12]), however further space can be saved by dispensing with the central solenoid, as well as not having an inboard breeding blanket. Both of these design choices present their own challenges in terms of start-up and the tritium breeding ratio, and PROCESS retains the capability to have them if required.

2.2. Centrepost

The default spherical tokamak toroidal field coil magnet model in PROCESS is a water-cooled copper centrepost, linked to copper return limbs. PROCESS retains the capability to use low and high temperature superconductors, however these follow the conventional aspect ratio model described in [8] and are individual coils instead joining onto a single centrepost. No model for a superconducting centrepost, such as that proposed by [13], is currently implemented. Joints are not accounted for in either the resistive or superconducting models and shielding is considered separately in the radial build.

The water-cooled copper centrepost is tapered in shape. It is straight from the ends to the height of the plasma, before reducing in thickness to its thinnest point at the midplane following an arc. The maximum radius is at a height level with the plasma x-point and is given by:

$$r_{top} = R - \delta a - 3\Delta_{SoL} - \Delta_{FW} \tag{1}$$

where R and a are the major and minor radius of the plasma, δ is the plasma triangularity and Δ_{SoL} is the thicknesses of the scrape-off layer (with the factor three accounting for flux expansion) and Δ_{FW} is the thicknesses of the first wall.

The resistivity of the centrepost is temperature dependent and is parameterised in the range of interest by:

$$\rho = 10^{-8}(1.72 + 0.0039T_{av})/0.92 \tag{2}$$

where T_{av} is the average temperature of the centrepost and the factor 0.92 corresponds to Glidcop [9]. The average temperature of the centrepost is given by:

$$T_{av} = T_{in} + \Delta T_{io}/2 + \Delta T_{film} + \Delta T_{con} \tag{3}$$

where T_{in} is the inlet coolant temperature (typically 40 °C), ΔT_{io} is the temperature rise in the coolant, ΔT_{film} is the temperature rise across the coolant/tube film boundary and ΔT_{con} is the temperature difference in the conductor. These are given by:

$$\Delta T_{io} = \frac{P_{tot}}{\rho_{H_2O} v_{av} A_{cool} C_{P_{H_2O}}} \tag{4}$$

where ρ_{H_2O} is the density of water, v_{av} the average coolant flow speed, A_{cool} the coolant cross-sectional area and $C_{P_{H_2O}}$ the specific heat capacity of water.

The total power (P_{tot}) is given by the sum of the resistive and nuclear heating. The nuclear heating is approximated by assuming a point source at the centre of the plasma. The fraction of neutrons hitting the centrepost is determined from the solid angle and an average path length of the centrepost diameter at the midplane, with an e-folding length of 0.08 m, is assumed for absorption.

The temperature rise across the coolant/tube film boundary is given by:

$$\Delta T_{film} = \frac{P_{tot}}{h 2\pi r_{cool} n_{cool} l_{cool}} \tag{5}$$

where r_{cool} is the radius of a coolant tube, n_{cool} is the number of coolant tubes and l_{cool} is the length of the coolant channels. These are being used to determine the surface area of all the tubes. h is given by:

$$h = \frac{N_u k_{H_2O}}{d_{cool}} \tag{6}$$

where d_{cool} is the coolant channel diameter, k_{H_2O} is the thermal conductivity of water and N_u is the Nusselt number; given by $0.023R_n^{0.8}P_{rnd}^{0.3}$ where R_n is the Reynolds number ($= \rho_{H_2O} v_{max} d_{cool}/\mu_{H_2O}$) and P_{rnd} the Prandlt number ($= C_{P_{H_2O}}\mu_{H_2O}/k_{H_2O}$). μ_{H_2O} here corresponds to the dynamic viscosity of water.

Finally, the temperature gradient in the conductor is estimated using an average distance between the coolant tubes [9]. The average temperature difference in the copper is:

$$\Delta T_{con} = \left(\frac{P_{tot}}{2k_{cp}V_{cp}(r_0^2 - r_{cool}^2)}\right)f_r \tag{7}$$

where k_{cp} is the centrepost thermal conductivity which is taken as a constant, V_{cp} is the centrepost volume, r_0 is the average distance between coolant tubes and:

$$f_r = r_{cool}^2 r_0^2 - 0.25r_{cool}^4 - 0.75r_0^4 + r_0^4\ln(r_0/r_{cool}) \tag{8}$$

The peak temperature in the centrepost is also computed in order that it is constrained to prevent weakening of the structure. This is given by:

$$T_{max} = T_{in} + \Delta T_{io} + \Delta T_{film} + \Delta T_{con-max} \tag{9}$$

where:

$$\Delta T_{con-max} = \frac{P_{tot}}{2k_{cp}V_{cp}}\left[\frac{r_{cool}^2 - r_0^2}{2} + r_0^2\ln(r_0/r_{cool})\right] \tag{10}$$

The pump power is calculated, to be added to the recirculating power, and is given by:

$$P_{pump} = \frac{\Delta P A_{cool} v_{max}}{\eta_{pump}} \tag{11}$$

where v_{max} is the peak flow speed at the midplane ($v_{av} = v_{max}(A_{mid}/A_{av})$ where A_{mid} is the cross-sectional area of the centrepost midplane and A_{av} is the average centrepost cross-sectional area), η_{pump} is the pump efficiency and ΔP is the pressure drop through the pipe given by:

$$\Delta P = f_{fric}\frac{l_{cool}}{d_{cool}}\rho_{H_2O}\frac{v_{max}^2}{2} \tag{12}$$

f_{fric} is the friction factor and is taken from [14]:

$$f_{fric} = \left(-2\log\left\{\frac{r_{gh}}{3.7} - \frac{5.02}{R_n}\log\left[\frac{r_{gh}}{3.7} + \frac{14.5}{R_n}\right]\right\}\right)^{-2} \tag{13}$$

where the roughness factor is estimated as $r_{gh} = 4.6 \times 10^{-5}/d_{cool}$.

The required inlet pressure is also calculated to guarantee that the pressure in the tubes remains below the saturation pressure. The saturation pressure is calculated from a fit to [15] using the peak coolant temperature:

$$T_{cool-max} = T_{in} + \Delta T_{io} + \Delta T_{film} + T_{marg} \tag{14}$$

where T_{marg} is the temperature margin taken as 10 °C.

2.3. Divertor

One of the largest challenges for spherical tokamaks is handling the high exhaust heats generated in the divertor. Detailed modelling of divertor configurations remains highly uncertain, and experimental campaigns with the new MAST-U Super-X divertor [16] have yet to be conducted. Therefore very simplified models are adopted here and their results are treated with caution.

For spherical tokamaks we use a double-null configuration to spread the heatload to the top and bottom and to minimise the power on the inboard side. PROCESS has previously considered double-null configurations geometrically, and recently a simple power sharing model has also been added [17]. The default spherical tokamak divertor model comes from [10] and is a closed divertor with a gaseous target that uniformly radiates within the divertor volume. The heat load on the wall is calculated, however based on the idealised assumption of uniform radiation these values are low. Realistically this model is used for space allocation in the build and a limit to P_{sep}/R or $P_{sep}B_t/qAR$ is applied to define the allowable heat.

2.4. Plasma shaping

For stability the following options are available for setting the elongation (κ), triangularity (δ) and minimum "edge" safety factor ($\bar{q}$) based on [11]:

$$\kappa_x = 2.05(1.0 + 0.44\epsilon^{2.1}) \tag{15}$$

$$\delta_x = 0.53(1.0 + 0.77\epsilon^3) \tag{16}$$

$$\bar{q}_{min} = 3.0(1.0 + 2.6\epsilon^{2.8}) \tag{17}$$

where $\epsilon = a/R = 1/A$ is the inverse aspect ratio. These equations are illustrated in Fig. 1, however their use does not have to be enforced. The lower limit on $\bar{q}$ is linked to the plasma current relation of [11], and the shape parameters have been obtained for PF coils inside the TF coil.

From the conventional aspect ratio tokamaks, PROCESS already enforces a β-limit. This value is set by the user and is significantly higher for spherical tokamaks; $\beta_N < 6$ is indicated by [2].

2.5. Plasma current

PROCESS calculates the plasma current based on a relation with the plasma shape and edge safety factor. For conventional aspect ratio tokamaks the ITER Physics Design Guidelines: 1989 [18] are used, however at tight aspect ratios this relation no longer holds. As described in [6], for spherical tokamaks the poloidal field becomes comparable with, or larger than, the toroidal field in the outboard region, and the toroidal and poloidal fields are comparable in the inboard region. Meanwhile, the toroidal circumference is comparable to the poloidal circumference in the outboard region, but is shorter in the inboard region. This leads to highly pitched field lines in the outboard region resulting in only a small amount of toroidal rotation, but moderately pitched field lines in the inboard region resulting in a large amount of toroidal rotation. The overall result is a strongly enhanced total toroidal rotation for a given plasma current, or stated another way, a higher plasma current for a given safety factor. Hence the need for an alternative relation that captures the enhancement of I_p/aB_t.

Peng, Galambos and Shipe [11] proposed such a relation for double-null D-shaped plasmas with $R/a < 3$:

$$I_p = \frac{5\kappa aB_t}{2\pi^2\bar{q}}(F_1 + F_2)\left(\frac{\arcsin(E_1)}{E_1} + \frac{\arcsin(E_2)}{E_2}\right) \tag{18}$$

where F_1 and F_2 are functions of κ_x, δ_x and ϵ, and E_1 and E_2 are functions of κ_x and δ_x that have not been reproduced here for brevity, but can be found in [11]. $\bar{q}$ is the "edge" safety factor and is related to q_{95} through:

$$q_{95} = 1.3\bar{q}(1.0 - \epsilon)^{0.6} \tag{19}$$

To investigate the applicability of Eq. (18) we created a series of free boundary equilibria using the code FIESTA. In Fig. 2 we calculate the plasma current using Eq. (18) and compare it to the value obtained from FIESTA. For the low elongation equilibria, the calculated values for the plasma current are close to those from FIESTA, however moving to higher elongations causes an underestimate by up to 20 per cent.

Given the parameter dependencies illustrated in Fig. 2 we chose to generate a new plasma current relation based on fits to our FIESTA equilibria. From [19], the plasma current for a large aspect ratio circular cross-section is given by:

$$I_p = \frac{2\pi a^2 B_t}{\mu_0 R q} \tag{20}$$

The assumptions of large aspect ratio and circular cross-section can be broken by adding functions of ϵ, κ and δ. We apply simple power laws giving the following equation to fit to the equilibria:

$$I_p = \left(\frac{a^2 B_t}{Rq_{95}}\right)c_1(1.0 + c_2\epsilon^{c_3})\kappa_x^{c_4}\delta_x^{c_5} \tag{21}$$

Fitting Eq. (21) to the equilibria using a non-linear least squares method we find $c_1 = 2.690$, $c_2 = 2.440$, $c_3 = 2.736$, $c_4 = 2.154$ and $c_5 = 0.060$. This fit is illustrated in Fig. 3 which shows that there is no bias with any parameter fitted and that the fit is accurate to 10 per cent.

Eqs. (18) and (21) are expressed in terms of the x-point elongation and triangularity. The linear relation between these and the 95% values expressed in [7] does not hold at high values of elongation and triangularity, and we will investigate this further in future work.

By default spherical tokamaks modelled using PROCESS are designed to operate in steady state. The plasma current is composed of the driven component, the bootstrap fraction and the diamagnetic fraction. For spherical tokamaks we use the Wilson model [20] to calculate the bootstap fraction and take the diamagnetic fraction as:

$$f_{dia} = \frac{\beta}{2.8} \tag{22}$$

based on fitting. Given the higher values of β achieved in a spherical tokamak, the diamagnetic fraction is more significant than in a conventional aspect ratio where we use the Sauter bootstrap model [21] by
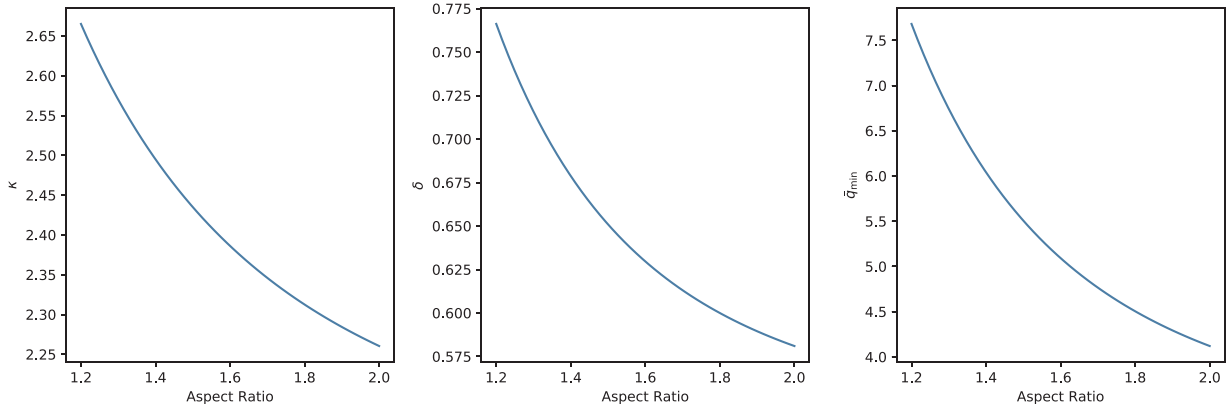

Fig. 1. The elongation (left), triangularity (middle) and safety factor (right) with aspect ratio as recommended by [11] for stability.
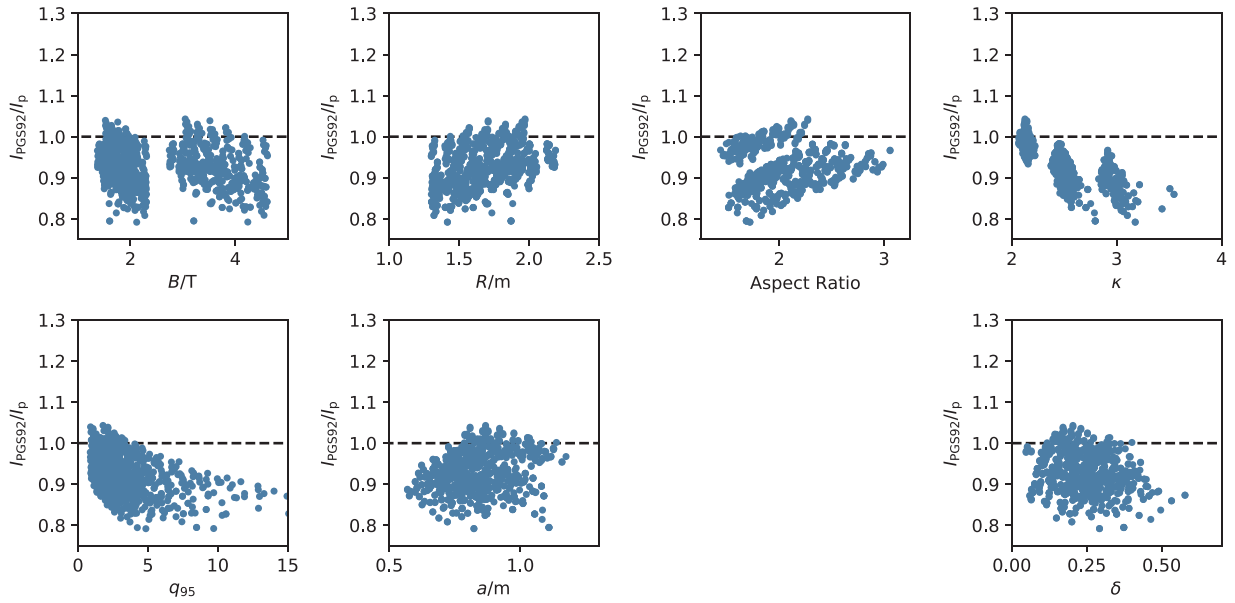
Fig. 2. The ratio of the predicted plasma current from Eq. (18) [11] to the value from the free boundary equilibria code FIESTA. Each panel plots the equilibria against a different dependency.

default and neglect the diamagnetic current.

The ratio of the plasma current to the current in the centrepost can be restricted to prevent disruptions using the constraint:

$$\frac{I_{\mathrm{p}}}{I_{\mathrm{cp}}} < 1.0 + 4.91(\epsilon - 0.62) \tag{23}$$

however this leads to ratios above one at aspect ratios below ~ 1.6, and therefore we usually restrict this ratio further.

2.6. Poloidal field

The average poloidal field at the plasma edge is given by [11] as:

$$B_{\mathrm{p}} = B_{\mathrm{t}} \frac{F_1 + F_2}{2\pi \bar{q}} \tag{24}$$

where F_1 and F_2 are the same functions of κ, δ and ϵ from Section 2.5. This replaces using Ampère's law with the perimeter of the plasma.

2.7. Poloidal field coils

A simple resistive PF coil model was proposed in [6] that takes advantage of the natural elongation of spherical plasmas and the typical shapes associated with the relations described in Section 2.4 and Fig. 1. A pair of coils are positioned top and bottom for shaping (SF), and in the vertical build these are located inboard of the TF coil. No assessment of nuclear heating is currently made on these coils. A second pair of coils are located radially outside the TF coil and are used to generate the vertical field (VF). Their currents are set by:

$$I_{\mathrm{SF}} = 0.3 A^{1.6} I_{\mathrm{p}} \tag{25}$$
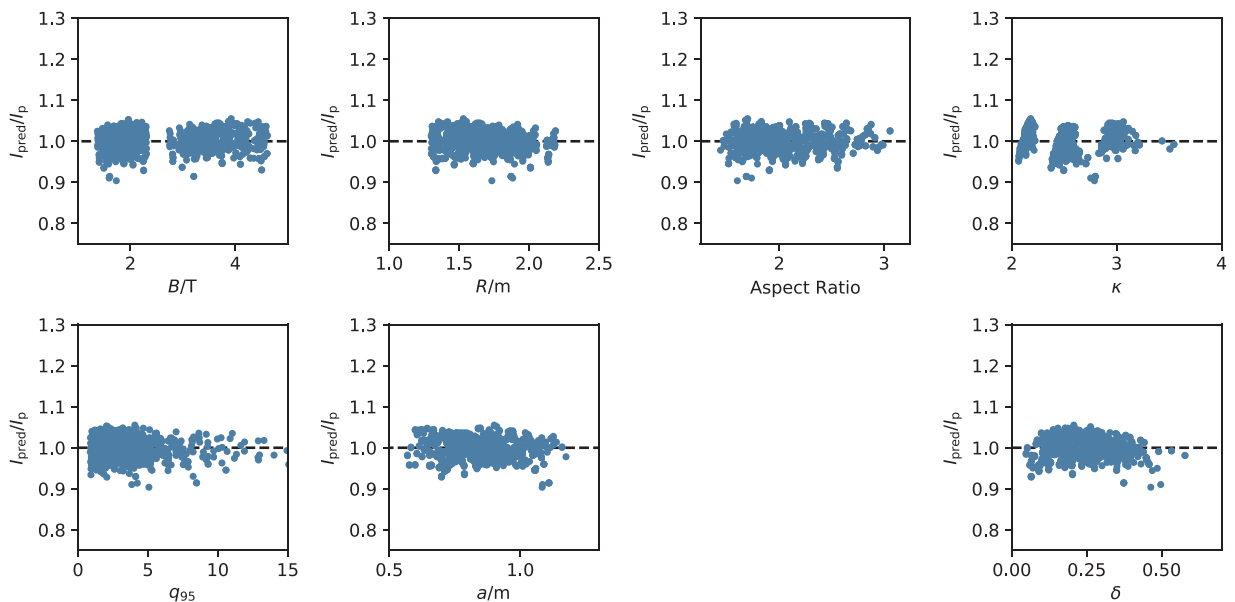

Fig. 3. The ratio of the predicted plasma current from Eq. (21) to the value from the free boundary equilibria code FIESTA. Each panel plots the equilibria against a different dependency. The four panels on the left represent variables where the underlying formula from [19] has not been modified while the three variables on the right have been added using fitting to FIESTA equilibria.

Table 1
Selected parameters for FNSF from PROCESS compared to those given in reference [22].

Parameter	Ref	PROCESS
Major radius, R (m)	1.70	1.70
Aspect ratio, $A = R/a$	1.75	1.75
Elongation, κ	2.75	2.75
Triangularity, δ	0.5	0.5
Fusion power, P_{fus} (MW)	162	162
Auxiliary power, P_{aux} (MW)	80	80
Toroidal field, B_T (T)	3.0	3.0
Plasma current, I_p (MA)	8.9	9.4
Normalised beta, β_N	5.5	4.5
H-factor, $H_{\text{IPB98}(y,2)}$	1.25	1.36
Greenwald fraction, n/n_{GW}	0.75	0.80

Table 2
Selected parameters for HTS-PP from PROCESS compared to those given in reference [24].

Parameter	Ref	PROCESS
Major radius, R (m)	3.0	3.0
Aspect ratio, $A = R/a$	2.0	2.0
Elongation, κ	2.5	2.5
Triangularity, δ	0.6	0.6
Fusion power, P_{fus} (MW)	500	500
Auxiliary power, P_{aux} (MW)	50	50
Toroidal field, B_T (T)	4.00	4.00
Plasma current, I_p (MA)	12	11
Normalised beta, β_N	4.00	3.85
H-factor, $H_{\text{IPB98}(y,2)}$	1.8	1.5
Greenwald fraction, n/n_{GW}	0.8	0.9

$$I_{\text{VF}} = -0.4 I_p \tag{26}$$

The conventional superconducting model can also be used that positions all the coils outside of the TF coil.

3. Benchmarking

In order to benchmark our models to test their applicability, we have chosen to compare with the proposed Fusion Nuclear Science Facility (FNSF) and a High Temperature Superconducting Pilot Plant (HTS-PP) described in [22–24].

3.1. Fusion nuclear science facility (FNSF)

FNSF is a proposed $R = 1.7$ m, $A = 1.75$ and $P_{\text{fus}} = 162$ MW device with resistive TF coils that will provide a nuclear environment to develop fusion materials and components [22]. In Table 1 we list some of the key parameters and compare them to our PROCESS run. This was performed using xenon seeding in PROCESS giving $P_{\text{sep}}/R = 17.5$ MW m^{-1}.

Overall PROCESS reproduces FNSF well, however the most noticeable difference is the plasma current. PROCESS finds a higher plasma current and lower safety factor, and this remains regardless of whether Eq. (18) or (21) is used to calculate it. Running PROCESS with Eq. (18) instead of (21) yields the same plasma current, but a lower safety factor to achieve it.

We have performed this run using the water-cooled centrepost model described in Section 2.2. The model finds an average temperature in the centrepost of 73 °C with a resistive loss of 92 MW, nuclear heating of 18 MW, and a required pumping power of 0.7 MW.

3.2. High temperature superconducting pilot plant (HTS-PP)

HTS-PP is a proposed $R = 3.0$ m, $A = 2$ and $P_{\text{fus}} = 500$ MW device, with HTS TF coils, that has a high neutron fluence and will be tritium and electrically self-sufficient [22]. In Table 2 we list some of the key parameters and compare them to our PROCESS run. This was performed using xenon seeding in PROCESS giving $P_{\text{sep}}/R = 20.0$ MW m^{-1}. The main disagreement is again the plasma current, however this time PROCESS finds a lower value. The H-factor is also lower for the PROCESS run.

HTS-PP highlights the need for efficiency gains for low fusion power plants to be viable. Taking the energy multiplication in the blanket as 1.269 and a thermal-to-electric conversion efficiency of 0.375, which are typical for EUROfusion-DEMO, then the gross electrical power is only 238 MW. With a neutral beam wall plug efficiency of 0.3, the auxiliary power system alone is using 167 MW; leaving very little to power the rest of the device, let alone produce the target 100 MW net electric output [24].

4. Conclusions

In this paper we have presented the spherical tokamak specific models in PROCESS. These include alternative relations for the plasma current, one of which is presented here for the first time. Additionally we have detailed a water-cooled copper centrepost model for the TF coil system. We have applied PROCESS to two reference cases to demonstrate their impact, illustrating the need to accurately predict the plasma current required. This is important, especially for small machines, as it will impact the amount of auxiliary current drive required and in turn the recirculating power, and hence the net electrical output of any pilot power plant.

Efficiencies play a large role in dictating the required fusion power of a power plant. The net electric output can be defined based on a target market, whether that is a pilot plant, something comparable to a small modular reactor or a full scale power plant. However recirculating power does not scale linearly with fusion power and hence for smaller devices it is essential this is minimised. Identifying methods of operating at high confinement is an option, however if this is not achieved then maximising the thermal cycle efficiency is the only solution. Once the required fusion power for a given output is defined, only then can the material and exhaust challenges be identified that will set the size of the device.

Authors' contributions

Stuart I. Muldrew: Conceptualization, Methodology, Software, Validation, Formal analysis, Investigation, Writing – Original Draft, Writing – Review & Editing, Visualization

Hanni Lux: Conceptualization, Supervision, Project administration

Geof Cunningham: Methodology, Software, Validation, Investigation

Tim C. Hender: Conceptualization, Investigation, Writing – Review & Editing, Supervision

Sebastien Kahn: Software

Peter J. Knight: Conceptualization, Software

Bhavin Patel: Validation, Investigation

Garry M. Voss: Validation

Howard R. Wilson: Validation, Investigation, Writing – Review & Editing, Supervision, Funding acquisition

Conflicts of interest

The authors declare no conflicts of interest.

obtain further information on the data and models underlying this paper please contact PublicationsManager@ukaea.uk.

References

[1] D.C. Robinson, Plasma Phys. Control. Fusion 41 (3A) (1999) A143–A157.

[2] M. Ono, R. Kaita, Recent progress on spherical torus research, Phys. Plasmas 22 (4) (2015) 40501.

[3] R. Wenninger, R. Kembleton, C. Bachmann, W. Biel, T. Bolzonella, S. Ciattaglia, F. Cismondi, M. Coleman, A. Donné, T. Eich, E. Fable, G. Federici, T. Franke, H. Lux, F. Maviglia, B. Meszaros, T. Pütterich, S. Saarelma, A. Snickers, F. Villone, P. Vincenzi, D. Wolff, H. Zohm, The physics and technology basis entering European system code studies for DEMO, Nucl. Fusion 57 (1) (2017) 16011.

[4] J. Morris, V. Chan, J. Chen, S. Mao, M. Ye, Validation and sensitivity of CFETR design using EU systems codes, Fusion Eng. Des. 146 (2019) 574–577.

[5] S.I. Muldrew, H. Lux, V. Menon, R. Srinivasan, Uncertainty analysis of an SST-2 fusion reactor design, Fusion Eng. Des. 146 (2019) 353–356.

[6] Y.-K. Peng, D. Strickler, Nucl. Fusion 26 (6) (1986) 769–777.

[7] M. Kovari, R. Kemp, H. Lux, P. Knight, J. Morris, D. Ward, "PROCESS": a systems code for fusion power plants – Part 1: Physics, Fusion Eng. Des. 89 (12) (2014) 3054–3069.

[8] M. Kovari, F. Fox, C. Harrington, R. Kembleton, P. Knight, H. Lux, J. Morris, "PROCESS": a systems code for fusion power plants – Part 2: Engineering, Fusion Eng. Des. 104 (2016) 9–20.

[9] J. Galambos, STAR Code: Spherical Tokamak Analysis and Reactor Code, Internal Oak Ridge Document, 1990.

[10] Y.-K. Peng, J. Hicks, Engineering feasibility of tight aspect ratio tokamak (spherical torus) reactors, 16th Symposium on Fusion Technology (1990).

[11] Y.-K.M. Peng, J.D. Galambos, P.C. Shipe, Small tokamaks for fusion technology testing, Fusion Technol. 21 (3P2A) (1992) 1729–1738.

[12] G. Voss, S. Davis, A. Dnestrovskij, A. Kirk, P. Knight, M. Loughlin, M. O'Brien, D. Sychugov, A. Tabasso, H. Wilson, Conceptual design of a component test facility based on the spherical tokamak, Fusion Eng. Des. 83 (10) (2008) 1648–1653.

[13] A. Sykes, A. Costley, C. Windsor, O. Asunta, G. Brittles, P. Buxton, V. Chuyanov, J. Connor, M. Gryaznevich, B. Huang, J. Hugill, A. Kukushkin, D. Kingham, A. Langtry, S. McNamara, J. Morgan, P. Noonan, J. Ross, V. Shevchenko, R. Slade, G. Smith, Nucl. Fusion 58 (1) (2017) 16039.

[14] Ž. Olujić, Compute friction factors fast for flow in pipes, Chem. Eng. 14 (1981) 91.

[15] J. Keenan, F. Keyes, P. Hill, J. Moore, Steam Tables: Thermodynamic Properties of Water, Including Vapor, Liquid, and Solid Phases, Wiley, 1969.

[16] G. Fishpool, J. Canik, G. Cunningham, J. Harrison, I. Katramados, A. Kirk, M. Kovari, H. Meyer, R. Scannell, Mast-upgrade divertor facility and assessing performance of long-legged divertors, J. Nucl. Mater. 438 (2013) S356–S359.

[17] A. Pearce, R. Kembleton, M. Kovari, H. Lux, F. Maviglia, J. Morris, M. Siccinio, Systems studies of double null divertor models, 46th EPS Conference on Plasma Physics (2019).

[18] N.A. Uckan, ITER Physics Group, ITER Physics Design Guidelines: 1989, International Atomic Energy Agency, 1990 IAEA/ITER/DS/10.

[19] J. Wesson, Tokamaks, Fourth Ed., Oxford University Press, 2011.

[20] H. Wilson, Nucl. Fusion 32 (2) (1992) 257–263.

[21] O. Sauter, C. Angioni, Y.R. Lin-Liu, Neoclassical conductivity and bootstrap current formulas for general axisymmetric equilibria and arbitrary collisionality regime, Phys. Plasmas 6 (7) (1999) 2834–2839.

[22] J. Menard, T. Brown, L. El-Guebaly, M. Boyer, J. Canik, B. Colling, R. Raman, Z. Wang, Y. Zhai, P. Buxton, B. Covele, C. D'Angelo, A. Davis, S. Gerhardt, M. Gryaznevich, M. Harb, T. Hender, S. Kaye, D. Kingham, M. Kotschenreuther, S. Mahajan, R. Maingi, E. Marriott, E. Meier, L. Mynsberge, C. Neumeyer, M. Ono, J.-K. Park, S. Sabbagh, V. Soukhanovskii, P. Valanju, R. Woolley, Nucl. Fusion 56 (10) (2016) 106023.

[23] J. Menard, Compact steady-state tokamak performance dependence on magnet and core physics limits, Philos. Trans. R. Soc. A: Math. Phys. Eng. Sci. A377 (2019) 20170440.

[24] J. Menard, R. Majeski, M. Ono, N. Bakharev, V. Gusev, M. Gryaznevich, D. Kingham, S. McNamara, P. Thomas, K. Hanada, J. Harrison, B. Lloyd, Y. Hwang, B. Lipschultz, H. Wilson, Y. Nagayama, Y. Ono, Y. Takase, M. Reinke, K. Tobita, Z. Gao, F. Alladio, R. Fonck, Fusion energy development applications utilizing the spherical tokamak and associated research needs and tools, 27th IAEA FEC (2018).